Layered cobalt oxide epitaxial films exhibiting thermoelectric ZT = 0.11 at room temperature

Yugo Takashima,[a] Yu-qiao Zhang,*[b] Jiake Wei,[c,d] Bin Feng,[c] Yuichi Ikuhara,[c,d] Hai Jun Cho,[a,b] and Hiromichi Ohta*[a,b]

Author affiliations

* Corresponding authors

[a]Graduate School of Information Science and Technology, Hokkaido University, N14W9, Kita, Sapporo 060−0814, Japan

[b]Research Institute for Electronic Science, Hokkaido University, N20W10, Kita, Sapporo 001−0020, Japan

E-mail: yuqiaozhang0730@gmail.com

E-mail: hiromichi.ohta@es.hokudai.ac.jp

[c]Institute of Engineering Innovation, The University of Tokyo, 2−11−16 Yayoi, Bunkyo, Tokyo 113−8656, Japan

[d]Elements Strategy Initiative for Structural Materials, Kyoto University, Yoshida-honmachi, Sakyo-ku, Kyoto 606−8501, Japan

Yu-qiao Zhang ORCiD: orcid.org/ 0000-0001-7579-4923

Bin Feng ORCiD: orcid.org/0000-0002-4306-2979

Yuichi Ikuhara ORCiD: orcid.org/0000-0003-3886-005X

Hai Jun Cho ORCiD: orcid.org/0000-0002-8642-4183

Hiromichi Ohta ORCiD: orcid.org/0000-0001-7013-0343

Keywords: layered cobaltite, $Ba_{1/3}CoO_2$, thermoelectric, ion substitution, thermal conductivity

Abstract

Among many thermoelectric materials, oxide-based materials draw significant interest due to their environmental compatibility. In particular, layered cobaltite, $Na_{0.75}CoO_2$, shows a large thermoelectric power factor parallel to the layers. However, the thermal conductivity (κ) is rather high (5−7 W m^{-1} K^{-1}), and therefore, its thermoelectric figure of merit *ZT* is small (~0.03) at room temperature. Here we show that substituting Na^+ ion with Ba^{2+} ion in Na_xCoO_2 drastically reduces the κ while keeping the large power factor, resulting in a large enhancement in *ZT*. We fabricated epitaxial films of $Na_{0.75}CoO_2$ by reactive solid-phase epitaxy method and performed ion-exchange treatment from Na^+ to Ba^{2+} to synthesize $Ba_{0.27}CoO_2$ films. The room temperature electrical conductivity (σ), thermopower (*S*), and power factor of the *c*-axis oriented $Ba_{0.27}CoO_2$ films along the in-plane direction were 2310 S cm^{-1}, +72 μV K^{-1}, and 1.2 mW m^{-1} K^{-2}, respectively, while the κ along the in-plane, which was clarified by

measuring the κ of the *c*-axis inclined (55°) film, was 3.3 W m^{-1} K^{-1}. This yields a *ZT* (= $S^2 \cdot \sigma \cdot T \cdot \kappa^{-1}$) value along the in-plane as high as 0.11 at room temperature, which is the highest among the oxide thermoelectric materials except oxychalcogenide, (BiO)(CuSe).

Introduction

Thermoelectric devices convert a temperature difference into electric current and vice versa, from the Seebeck effect/Peltier effect.[1, 2] Since thermoelectric devices can convert wasted heat exhausted in our daily life into electricity, it has attracted increasing attention as a potential solution for the realization of affordable and clean energy in Sustainable Development Goals (SDGs).[3, 4] Previously, wasted heat from large-scale high-temperature environments, like factories, thermal power plants, and automobiles, has been targeted for the thermoelectric conversion. Therefore, thermoelectric materials exhibiting a large figure of merit (*ZT*) at high-temperature (800−1000 K) have been developed proactively.[5-8] Nevertheless, thermoelectric conversion of small-scale exhausted heat from computers, stoves, sunlight, and our body is also important for the realization of SDGs. Thus, thermoelectric materials exhibiting a large *ZT* around room temperature are also required.

Further, thermoelectric materials must avoid the use of rare and toxic elements since economic and environmental viabilities are of great concern in future. Therefore, although layered bismuth telluride based thermoelectric materials exhibit large *ZT* (= $S^2 \cdot \sigma \cdot T \cdot \kappa^{-1}$ = ~0.8[1], where *S*, σ, *T*, and κ are the thermopower, electrical conductivity, absolute temperature, and thermal conductivity) values at room temperature, they lack the sustainability due to the existence of Te, which is rare and a toxic. In this regard, oxide-based thermoelectric materials offer an excellent alternative due to their environmental compatibility.[9] Although it is known that oxychalcogenide (BiO)(CuSe)[10, 11] exhibits a large *ZT* ~0.2 at room temperature and ~1.4 at 650 °C, chemical instability under oxygen atmosphere at high temperature can potentially cause problems in real application. One of the most commonly addressed thermoelectric oxides, electron-doped $SrTiO_3$ and $Ca_3Co_4O_9$, exhibit large *ZT* values at elevated temperatures (*ZT* ~0.3 at 1000 K as the reliable value).[12, 13] However, the *ZT* values of these oxides are extremely small at room temperature (*ZT* ~0.05 for electron doped $SrTiO_3$, *ZT* ~0.04 for $Ca_3Co_4O_9$).[12] The origin of such low *ZT* observed from oxides at room temperature is their high κ. For example, $Na_{0.75}CoO_2$ shows a large thermoelectric power factor (PF = $S^2 \cdot \sigma$, 2.38 mW m^{-1} K^{-2}) along to the layers.[14] However, the κ is

rather high (~7 W m^{-1} K^{-1}), and therefore, the thermoelectric figure of merit *ZT* is small (~0.03[15, 16]) at room temperature.

In order to overcome this difficulty, we recently investigated the effect of the ion exchange from Na^+ ion to alkali earth ions on the κ of $Na_{0.75}CoO_2$.[17] Firstly, we fabricated $Na_{0.75}CoO_2$ epitaxial films by the reactive solid-phase (R-SPE) epitaxy method.[18-20] Then, the Na^+ ions were topotactically substituted with Ca^{2+} and Sr^{2+} ions by the conventional ion exchange treatment.[21-23] We measured the κ of the resultant epitaxial films of $Na_{0.75}CoO_2$, $Ca_{1/3}CoO_2$, and $Sr_{1/3}CoO_2$ using time-domain thermoreflectance (TDTR) method, and the result showed that the κ parallel to this layered structure can be reduced by substituting heavier elements between the CoO_2 planes, as schematically hypothesized in Fig. 1, whereas the κ normal to the layered structure was ~1.5 W m^{-1} K^{-1}, independent on the element mass.[17]

In this study, we focused on the substitution of Ba^{2+} because the atomic mass of Ba is the heaviest among alkali earth elements. The thermoelectric properties of $Ba_{1/3}CoO_2$ was addressed in few previous studies. Recently, Liu *et al*. fabricated Ba_xCoO_2 (x = 0.19, 0.28, 0.30, and 0.33) ceramic samples through the ion-exchange treatment of

Na_xCoO_2 ceramics and measured the thermoelectric properties.[24, 25] They showed that the resistivity (ρ), S, and κ of the Ba_xCoO_2 ceramics at room temperature were 4−30 mΩ cm (σ = 33−250 S cm^{-1}), ~+70 μV K^{-1}, and 3−5 W m^{-1} K^{-1}, respectively. Thus, the ZT of the Ba_xCoO_2 ceramics at room temperature was 0.012 at the largest. The PF was 0.12 mW m^{-1} K^{-2}, which is an order magnitude lower than that of the epitaxial films of $Na_{0.75}CoO_2$ (1.23 mW m^{-1} K^{-2}), $Ca_{1/3}CoO_2$ (1.08 mW m^{-1} K^{-2}), and $Sr_{1/3}CoO_2$ (1.18 mW m^{-1} K^{-2}), measured parallel to the layered structure,[17] which is probably due to carrier scattering at grain or domain boundaries. On the other hand, the lowest κ was 3 W m^{-1} K^{-1}, which is lower than that of the epitaxial films of $Na_{0.75}CoO_2$ (5.46 W m^{-1} K^{-1}), $Ca_{1/3}CoO_2$ (6.79 W m^{-1} K^{-1}), and $Sr_{1/3}CoO_2$ (4.51 W m^{-1} K^{-1}) (parallel to the layered structure).[17] From these points of view, we expected that $Ba_{1/3}CoO_2$ epitaxial films show an enhanced ZT parallel to the layered structure as their power factor is not significantly damaged by grain or domain boundaries.

Here we report that the $Ba_{1/3}CoO_2$ epitaxial films, which were fabricated by the ion exchange treatment of $Na_{0.75}CoO_2$ epitaxial films exhibit significantly low κ while maintaining the large power factor and show rather large ZT = 0.11 at room

temperature. This value is the highest among the oxide thermoelectric materials except oxychalcogenide, (BiO)(CuSe).

Experimental

Preparation of $Na_{0.75}CoO_2$ epitaxial films. We prepared $Ba_{1/3}CoO_2$ epitaxial films as schematically summarized in Fig. 2, which also shows the crystal structures of CoO, $Na_{0.75}CoO_2$, and $Ba_{1/3}CoO_2$. $Na_{0.75}CoO_2$ epitaxial films were prepared on α-Al_2O_3 substrates by the reactive solid-phase epitaxy (R-SPE) method.[18-20] First, CoO films were heteroepitaxially grown on (0001) or (1-100) α-Al_2O_3 single-crystal substrates (10 mm × 10 mm × 0.5 mm) at 700 °C in an oxygen atmosphere (10^{-3} Pa) by pulsed laser deposition technique (KrF excimer laser, ~2 J cm^{-2} $pulse^{-1}$, 10 Hz). Then, the surface of the CoO film was heated at 750 °C in air with $NaHCO_3$ powder. In order to keep the film surface clean, the yttria stabilized zirconia (YSZ) single crystal plate (10 mm × 10 mm × 0.5 mm) was put on the film surface during the heating. Detailed preparation process of $Na_{0.75}CoO_2$ epitaxial films is described elsewhere.[18-20]

Ion exchange from Na^+ to Ba^{2+}. The ion exchange from Na^+ to Ba^{2+} was performed by heating the $Na_{0.75}CoO_2$ epitaxial films with molten $Ba(NO_3)_2$ and KNO_3 at 500 °C in an

alumina crucible for 1 h. After the ion exchange treatment, the resultant films were washed with distilled water. These processes were similar to the process used to prepare $Sr_{1/3}CoO_2$ and $Ca_{1/3}CoO_2$ epitaxial films by the ion exchange of $Na_{0.75}CoO_2$ epitaxial films.[22, 23]

Crystallographic characterization of the films. The crystallographic characteristics including the thickness, orientation, and lattice parameters of the resultant films were analyzed using the high-resolution X-ray diffraction (HR-XRD, Cu $K\alpha_1$ radiation, ATX-G, Rigaku Co.). Out-of-plane Bragg diffraction patterns, in-plane Bragg diffraction patterns, rocking curves, and X-ray reflection patterns were acquired. The surface morphologies of the resultant films were observed by a scanning probe microscopy (SPM, Nanocute, Hitach High-Tech Sci. Co.). Topographic atomic force microscope (AFM) images (2 μm × 2 μm) were acquired. The atomic arrangement of the resultant films was visualized using high-angle annular dark-field scanning transmission electron microscopy (HAADF-STEM).

Measurements of the electrical conductivity and thermopower. The electrical conductivity of the resultant films was measured by dc four-probe method in van der

Pauw electrode configuration. The thermopower of the resultant films was measured by the conventional steady-state method. The film sample was placed on the gap (~5 mm) between two Peltier devices. By applying the forward/reverse current to each Peltier device, temperature differences were generated in the sample. We then measured the temperature difference (ΔT) and the thermo-electromotive force (ΔV) simultaneously at room temperature, and the thermopower was calculated as the linear slope of the ΔT – ΔV plot (Supplementary Fig. S1). Details of our thermopower measurement system are described elsewhere.[26, 27]

Measurements of the thermal conductivity. Cross-plane thermal conductivity (κ) of the resultant films was measured by the time domain thermo-reflectance (TDTR, PicoTR, PicoTherm Co.). 116-nm-thick Mo was deposited on the resultant films as a transducer by dc sputtering. The decay curves of the TDTR signals were simulated using the packaged software developed by PicoTherm Co. In our simulation, to minimize the number of free parameters, we used constant values for Mo transducers, including bulk density = 10000 kg m^{-3}, heat capacity (C_p) = 250 J Kg^{-1} K^{-1} and κ = 45.4 W m^{-1} K^{-1}. Details of our thermal conductivity measurement system are described elsewhere.[17, 28, 29]

Uncertainty in the *ZT* value. We fabricated more than 5 samples and we measured all samples. The uncertainty in the S and the σ were less than 5%, while that in the κ was ~15%. Therefore, the uncertainty in the ZT is approximated to be ~20%.

Results and discussion

Figure 3 summarizes the out-of-plane XRD patterns and the topographic atomic force microscope (AFM) images of the resultant CoO film (Figs. 3a and 3d), R-SPE grown $Na_{0.75}CoO_2$ film (Figs. 3b and 3e), and Ba^{2+} ion-exchanged film (Figs. 3c and 3f) grown on (0001) α-Al_2O_3 substrates. Only an intense Bragg peak of 111 CoO is seen together with 0006 α-Al_2O_3 substrate (Fig. 3a), indicating the strong (111) orientation in the CoO film. The full width at half maximum (FWHM) of the out-of-plane rocking curve (OXRC) of 111 CoO was ~0.02° (Supplementary Fig. S2a), which is almost as small as the resolution of our optical setup of the XRD. The thickness of the CoO film was 93 nm, which was evaluated using the Pendellösung fringes around the Bragg peak of 111 CoO. The heteroepitaxial growth with the relationship of (111)[1-10] CoO || (0001)[1-100] α-Al_2O_3 was confirmed by the in-plane XRD patterns (Supplementary Fig. S3a).

Triangle shaped facets are clearly seen in the topographic AFM image of the film (Fig. 3d), confirming the heteroepitaxial growth of CoO.

After the R-SPE treatment, only intense Bragg peaks of 000*l* $Na_{0.75}CoO_2$ are seen (Fig. 3b). The thickness of the $Na_{0.75}CoO_2$ film was 182 nm, roughly twice that of the CoO film. Although the FWHM of the OXRC of 0002 $Na_{0.75}CoO_2$ was ~0.6° (Supplementary Fig. S2b), hexagonal-shaped plate-like crystals with large terrace was observed in the topographic AFM image (Fig. 3e). Thus, the broadening of the FWHM of the OXRC indicates the bending of the $Na_{0.75}CoO_2$ crystal. The in-plane XRD pattern (Supplementary Fig. S3b) confirmed the heteroepitaxial growth of $Na_{0.75}CoO_2$ film on (0001) α-Al_2O_3 substrate with the epitaxial relationship of (0001)[11-20] $Na_{0.75}CoO_2$ || (0001)[1-100] α-Al_2O_3. After the Ba^{2+} ion exchange treatment, the Bragg peak position of 000*l* is shifted to the left, indicating a lattice expansion in the out-of-plane direction (Fig. 3c). The *c*-axis lattice parameter is 12.225 Å, which corresponds well with the reported value (12.2 Å[25]) of $Ba_{1/3}CoO_2$. The in-plane XRD pattern (Supplementary Fig. S3c) indicated that there are two ordering structures of Ba ions. The *a*-axis lattice parameter was calculated to be 2.829 Å. The topographic AFM image of the resultant film (Fig. 3f) is similar to that of the $Na_{0.75}CoO_2$ film.

Since the orientation of the films was inclined on (1-100) α-Al_2O_3 substrate, Bragg diffraction peaks were not observed in the out-of-plane Bragg patterns of the resultant CoO film, R-SPE grown $Na_{0.75}CoO_2$ film, and Ba^{2+} ion-exchanged film (data not shown). Figures 3g−3i show the topographic AFM images of the CoO (Fig. 3g), $Na_{0.75}CoO_2$ (Fig. 3h), and Ba^{2+} ion-exchanged (Fig. 3i) films grown on (1-100) α-Al_2O_3 substrate by the same way. Stripe patterns were seen in Figs. 3g−3i, which are similar to the surface of inclined films. The heteroepitaxial growth of CoO, $Na_{0.75}CoO_2$, and $Ba_{1/3}CoO_2$ films on (1-100) α-Al_2O_3 substrate was confirmed by the in-plane XRD patterns (Supplementary Fig. S4); [1-10] CoO || [0001] α-Al_2O_3, [11-20] $Na_{0.75}CoO_2$ || [0001] α-Al_2O_3, and [11-20] $Ba_{1/3}CoO_2$ || [0001] α-Al_2O_3.

To further clarify the orientation of the film and the atomic arrangement, we performed high-angle annular dark-field scanning transmission electron microscopy (HAADF-STEM) observation. Figures 4a and 4b show the cross-sectional HAADF-STEM images of the Ba^{2+} ion-exchanged films on (0001) α-Al_2O_3 substrate. The e-beam incident direction is along the [1-100] α-Al_2O_3. The layered atomic arrangement parallel to the substrate surface is clearly visualized (Fig. 4b and Supplementary Fig. S5a).

Approximately 10-nm-thick amorphous layer is also detected between the layered crystal and the substrate. Energy dispersive X-ray spectroscopy (EDS) results of the film (data not shown) revealed that the upper part of the film is composed of Ba, Co, and O. Signal from Na was negligible. The bottom amorphous part is composed of Ba, Al, and O. The concentration ratio of Ba/Co inside the film was about 0.27. These results show that the resultant film is $Ba_{0.27}CoO_2$.

On the other hand, an inclined layered structure was revealed in the HAADF-STEM images of the film on (1-100) α-Al_2O_3 substrate (Figs. 4c and 4d). The e-beam incident direction is along with the [0001] α-Al_2O_3. Similar to the $Ba_{0.27}CoO_2$ film on (0001) α-Al_2O_3 substrate, the layered atomic arrangement is clearly visualized. It should be noted that the layer is inclined 55° to the substrate surface. Although the interface amorphous layer is thick (15−30 nm), the crystal structure and the chemical composition of the layered crystal layer is similar to those of the $Ba_{1/3}CoO_2$ film on (0001) α-Al_2O_3 substrate. The inclined structure is consistent with the topographic AFM image (Fig. 3i).

Then, we measured the electrical conductivity (σ) and thermopower (S) parallel to the film surface of the (0001)-oriented $Ba_{0.27}CoO_2$ film grown on (0001) α-Al_2O_3 substrate

at room temperature. The σ was 2310 S cm^{-1}, the S was +72 μV K^{-1}, and the power factor (PF = $S^2 \cdot \sigma$) was 1.2 mW m^{-1} K^{-2}, respectively. The PF is the same (1.2 mW m^{-1} K^{-2}) with that of (0001)-oriented $Na_{0.75}CoO_2$ film grown on (0001) α-Al_2O_3 substrate at room temperature. Thus, Ba ion substitution does not affect the PF.

Next, we measured the thermal conductivity (κ) normal to the film surface of the $Ba_{0.27}CoO_2$ films grown on (0001) and (1-100) α-Al_2O_3 substrates by the TDTR method at room temperature. The κ of the $Ba_{0.27}CoO_2$ film on (0001) α-Al_2O_3 substrate was 1.3 W m^{-1} K^{-1} and that on (1-100) α-Al_2O_3 substrate was 2.8 W m^{-1} K^{-1}. In order to extract the κ of the parallel to the layered structure in $Ba_{0.27}CoO_2$ film, we used following equation as reported previously.[17]

$$\kappa_{obsd} = \sqrt{\kappa_{\parallel}^2 \cos^2\varphi + \kappa_{\perp}^2 \sin^2\varphi}$$

where φ, κ_{obsd}, $\kappa_{//}$ and $\kappa_{\perp}$ are the inclined angle of the layers to perpendicular of the film surface, the observed thermal conductivity, thermal conductivity parallel and perpendicular to the CoO_2 layers, respectively. Note that isotropy is recovered if $\kappa_{//} = \kappa_{\perp}$, and this equation can be applied both isotropic and anisotropic materials.[26] In the case of this study, $\varphi = 90 - 55 = 35°$, $\kappa_{\perp}$ =1.3 W m^{-1} K^{-1} and κ_{obsd} = 2.8 W m^{-1} K^{-1}, the

$\kappa_{//}$ was calculated to be 3.29 W m^{-1} K^{-1} (Supplementary Fig. S6), which is ~60% of that of $Na_{0.75}CoO_2$ epitaxial film as hypothesized.

Here we summarize and compare the thermoelectric properties of the $Ba_{0.27}CoO_2$ and $Na_{0.75}CoO_2$ films on (0001) α-Al_2O_3 substrate along with reported values for $Ca_{1/3}CoO_2$ and $Sr_{1/3}CoO_2$ [22, 23] (Fig. 5 and Supplementary Table S1). Although there are some differences in the in-plane electrical conductivity (σ_{ip}) (Fig. 5a) and thermopower (S_{ip}) (Fig. 5b) of $Ca_{1/3}CoO_2$, $Na_{0.75}CoO_2$, $Sr_{1/3}CoO_2$ and $Ba_{0.27}CoO_2$, the power factor PF_{ip} (Fig. 5c) was almost constant (1.08−1.2 mW m^{-1} K^{-2}) and does not show clear dependence on the atomic mass of A_x. The main difference was detected in the thermal conductivity (κ) (Fig. 5d). Although the out-of-plane thermal conductivity (κ_{op}) was almost independent on the atomic mass of A_x, the κ_{ip} drastically decreased from 6.79 W m^{-1} K^{-1} to 3.29 W m^{-1} K^{-1} with increasing the atomic mass of A_x from 13.2 ($Ca_{1/3}$) to 45.3 ($Ba_{1/3}$), resulting in a significant enhancement in ZT along with the layered structure. The resulting ZT_{in} was 0.11 at room temperature, which is the highest among the oxide thermoelectric materials except oxychalcogenide, (BiO)(CuSe).

Conclusions

In summary, we have shown that Ba^{2+} ion substitution with Na^{+} ion in $Na_{0.75}CoO_2$ significantly reduces the in-plane κ while keeping the large power factor, resulting in the large enhancement of *ZT*. We fabricated the epitaxial films of $Ba_{1/3}CoO_2$ from $Na_{0.75}CoO_2$ epitaxial films by ion-exchanging Na^{+} and Ba^{2+}. The σ, *S*, and power factor of the *c*-axis oriented $Ba_{1/3}CoO_2$ films along the in-plane were 2310 S cm^{-1}, +72 μV K^{-1}, and 1.2 mW m^{-1} K^{-2}, respectively. The κ along the in-plane, which was clarified by measuring the κ of the *c*-axis inclined (55°) film, was 3.29 W m^{-1} K^{-1}. The *ZT* along the in-plane was as large as 0.11 at room temperature, which is the highest among the oxide thermoelectric materials except oxychalcogenide, (BiO)(CuSe).

Acknowledgements

This research was supported by Grants-in-Aid for Innovative Areas (19H05791 and 19H05788) and Grants-in-Aid for Scientific Research A (17H01314) from the JSPS. A part of this work was supported by Dynamic Alliance for Open Innovation Bridging Human, Environment, and Materials, and by the Network Joint Research Center for Materials and Devices. A part of this work was conducted at Advanced Characterization Nanotechnology Platform of the University of Tokyo, supported by “Nanotechnology Platform” of the Ministry of Education, Culture, Sports, Science and Technology (MEXT), Japan, Grant Number JPMXP09A20UT0090. H.J.C. acknowledges the support from Nippon Sheet Glass Foundation for Materials Science and Engineering.

References

1. G. J. Snyder and E. S. Toberer, *Nature Mater.*, 2008, **7**, 105-114.
2. J. He and T. M. Tritt, *Science*, 2017, **357**, eaak9997.
3. D. Griggs, M. Stafford-Smith, O. Gaffney, J. Rockstrom, M. C. Ohman, P. Shyamsundar, W. Steffen, G. Glaser, N. Kanie and I. Noble, *Nature*, 2013, **495**, 305-307.
4. S. LeBlanc, *Sustain. Mater. Technol.*, 2014, **1-2**, 26-35.
5. K. Biswas, J. Q. He, I. D. Blum, C. I. Wu, T. P. Hogan, D. N. Seidman, V. P. Dravid and M. G. Kanatzidis, *Nature*, 2012, **489**, 414-418.
6. L. D. Zhao, G. J. Tan, S. Q. Hao, J. Q. He, Y. L. Pei, H. Chi, H. Wang, S. K. Gong, H. B. Xu, V. P. Dravid, C. Uher, G. J. Snyder, C. Wolverton and M. G. Kanatzidis, *Science*, 2016, **351**, 141-144.
7. K. F. Hsu, S. Loo, F. Guo, W. Chen, J. S. Dyck, C. Uher, T. Hogan, E. K. Polychroniadis and M. G. Kanatzidis, *Science*, 2004, **303**, 818-821.
8. Y. He, T. Day, T. S. Zhang, H. L. Liu, X. Shi, L. D. Chen and G. J. Snyder, *Adv. Mater.*, 2014, **26**, 3974-3978.
9. K. Koumoto, R. Funahashi, E. Guilmeau, Y. Miyazaki, A. Weidenkaff, Y. F. Wang and C. L. Wan, *Journal of the American Ceramic Society*, 2013, **96**, 1-23.
10. L. D. Zhao, J. Q. He, D. Berardan, Y. H. Lin, J. F. Li, C. W. Nan and N. Dragoe, *Energ Environ Sci*, 2014, **7**, 2900-2924.
11. J. H. Sui, J. Li, J. Q. He, Y. L. Pei, D. Berardan, H. J. Wu, N. Dragoe, W. Cai and L. D. Zhao, *Energ Environ Sci*, 2013, **6**, 2916-2920.
12. H. Ohta, K. Sugiura and K. Koumoto, *Inorg. Chem.*, 2008, **47**, 8429-8436.

13. J. W. Fergus, *J. Eur. Ceram. Soc.*, 2012, **32**, 525-540.

14. I. Terasaki, Y. Sasago and K. Uchinokura, *Phys. Rev. B*, 1997, **56**, 12685-12687.

15. B. C. Sales, R. Jin, K. A. Affholter, P. Khalifah, G. M. Veith and D. Mandrus, *Phys. Rev. B*, 2004, **70**, 174419.

16. K. Fujita, T. Mochida and K. Nakamura, *Jpn. J. Appl. Phys.*, 2001, **40**, 4644-4647.

17. H. J. Cho, Y. Takashima, Y. Nezu, T. Onozato and H. Ohta, *Adv. Mater. Interfaces*, 2019, **7**, 1901816.

18. H. Ohta, S. W. Kim, S. Ohta, K. Koumoto, M. Hirano and H. Hosono, *Cryst. Growth Des.*, 2005, **5**, 25-28.

19. H. Ohta, A. Mizutani, K. Sugiura, M. Hirano, H. Hosono and K. Koumoto, *Adv. Mater.*, 2006, **18**, 1649.

20. K. Sugiura, H. Ohta, S. Nakagawa, R. Huang, Y. Ikuhara, K. Nomura, H. Hosono and K. Koumoto, *Appl. Phys. Lett.*, 2009, **94**, 152105.

21. K. Sugiura, H. Ohta, Y. Ishida, R. Huang, T. Saito, Y. Ikuhara, K. Nomura, H. Hosono and K. Koumoto, *Appl. Phys. Express*, 2009, **2**.

22. K. Sugiura, H. Ohta, K. Nomura, M. Hirano, H. Hosono and K. Koumoto, *Appl. Phys. Lett.*, 2006, **89**, 032111.

23. K. Sugiura, H. Ohta, K. Nomura, M. Hirano, H. Hosono and K. Koumoto, *Appl. Phys. Lett.*, 2006, **88**, 082109.

24. J. Liu, X. Huang, D. Yang, S. Wan and G. Xu, *Scripta Mater.*, 2015, **100**, 63-65.

25. J. Liu, X. Huang, D. Yang, G. Xu and L. Chen, *Dalton Trans.*, 2014, **43**, 15414.

26. H. Ohta, S. W. Kim, S. Kaneki, A. Yamamoto and T. Hashizume, *Adv. Sci.*, 2018, **5**, 201700696.

27. H. Ohta, T. Mizuno, S. Zheng, T. Kato, Y. Ikuhara, K. Abe, H. Kumomi, K. Nomura and H. Hosono, *Adv Mater*, 2012, **24**, 740-744.

28. H. J. Cho, G. Kim, T. Onozato, H. Jeen and H. Ohta, *Int. J. Heat Mass Transf.*, 2019, **137**, 263-267.

29. Y. Isosaki, Y. Yamashita, T. Yagi, J. Jia, N. Taketoshi, S. Nakamura and Y. Shigesato, *J Vac Sci Technol A*, 2017, **35**.

Conflicts of interest

There are no conflicts to declare.

Author contributions

Y.T. and Y.Z. performed the sample preparation, measurements, and analyses. J.W., B.F., and Y.I. performed the STEM analyses. H.J.C. analyzed and interpreted the data. H.O. planned and supervised the project. All authors discussed the results and commented on the manuscript.

Footnote

† Electronic supplementary information (ESI) available. See DOI:

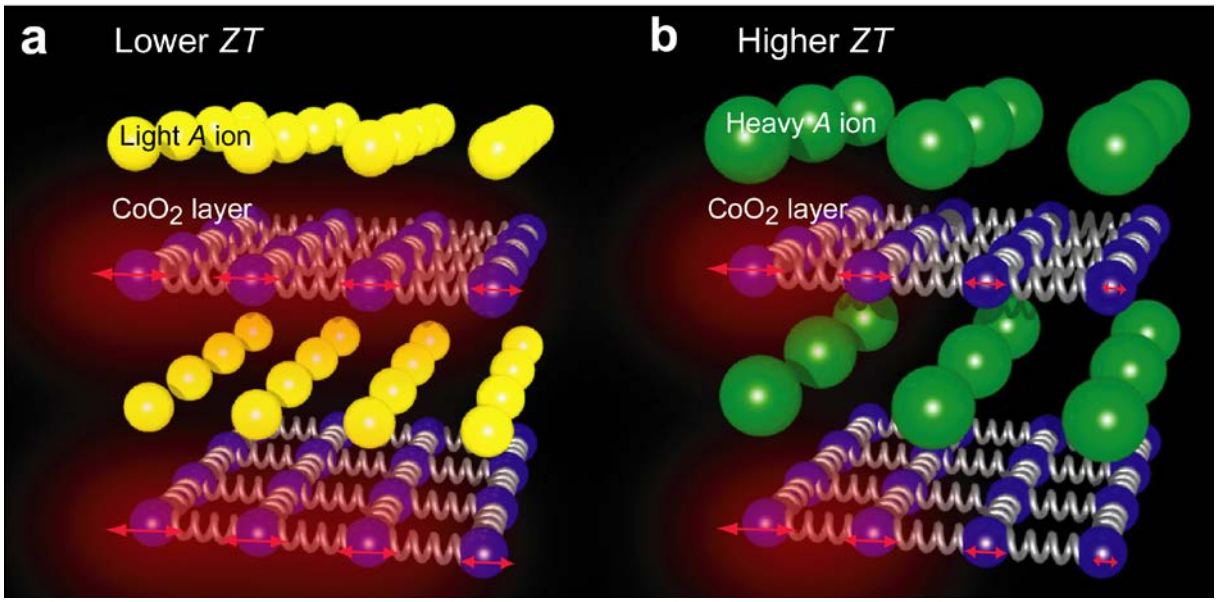

Figure 1. Hypothesis toward the *ZT* improvement of layered cobaltite, A_xCoO_2. We expected that the lattice vibration, indicated by red arrows of the rigid CoO_2 layer would be significantly suppressed by the substitution of *A* ion from (a) light one to (b) heavy one. If the substitution does not affect the power factor ($S^2 \cdot \sigma$), the *ZT* would be improved significantly by the substitution.

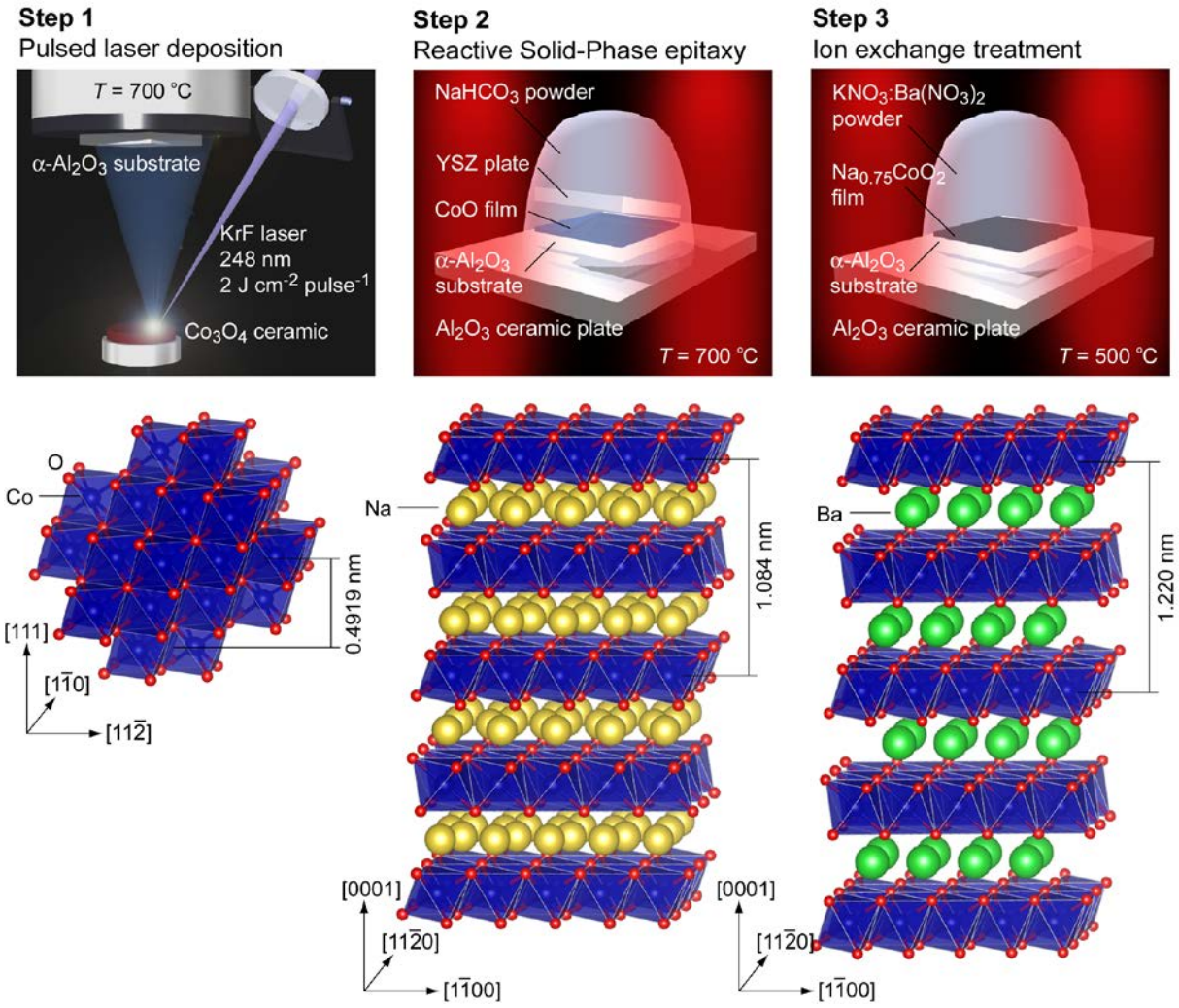

Figure 2. Fabrication procedure of $Ba_{1/3}CoO_2$ epitaxial films. Step 1: CoO epitaxial film growth by the pulsed laser deposition on α-Al_2O_3 substrates. Step 2: $Na_{0.75}CoO_2$ film growth by the Reactive Solid-Phase Epitaxy method. Step 3: Ion exchange treatment from Na to Ba. After the ion exchange treatment, the resultant film was washed by distilled water several times.

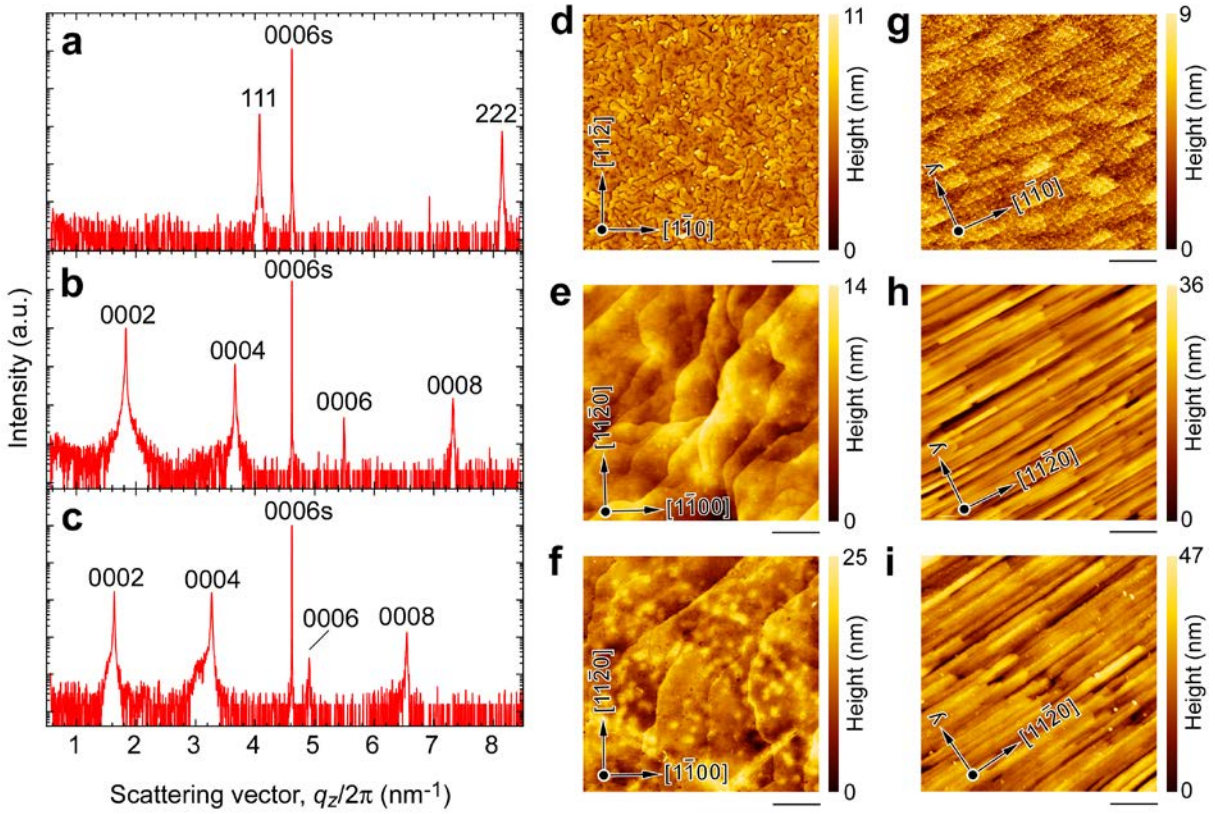

Figure 3. Crystal structural analyses of the resultant films. (a)−(c) Change in the out-of-plane XRD pattern of the resultant films grown on (0001) α-Al_2O_3 substrate (a) after step 1, (b) after step 2, and (c) after step 3. The crystalline phase of (a) is CoO (93 nm), (b) is $Na_{0.75}CoO_2$ (182 nm), and (c) is $Ba_{1/3}CoO_2$ (200 nm). (d)−(f) Topographic AFM images of the resultant films grown on (0001) α-Al_2O_3 substrate (a) after step 1 (CoO), (b) after step 2 ($Na_{0.75}CoO_2$), and (c) after step 3 ($Ba_{1/3}CoO_2$). (g)−(i) Topographic AFM images of the resultant films grown on (1-100) α-Al_2O_3 substrate (a) after step 1, (b) after step 2, and (c) after step 3. All the scale bars are 1 μm. Plate-like grains are seen in (d)−(f), whereas stripe patterns are seen in (g)−(i).

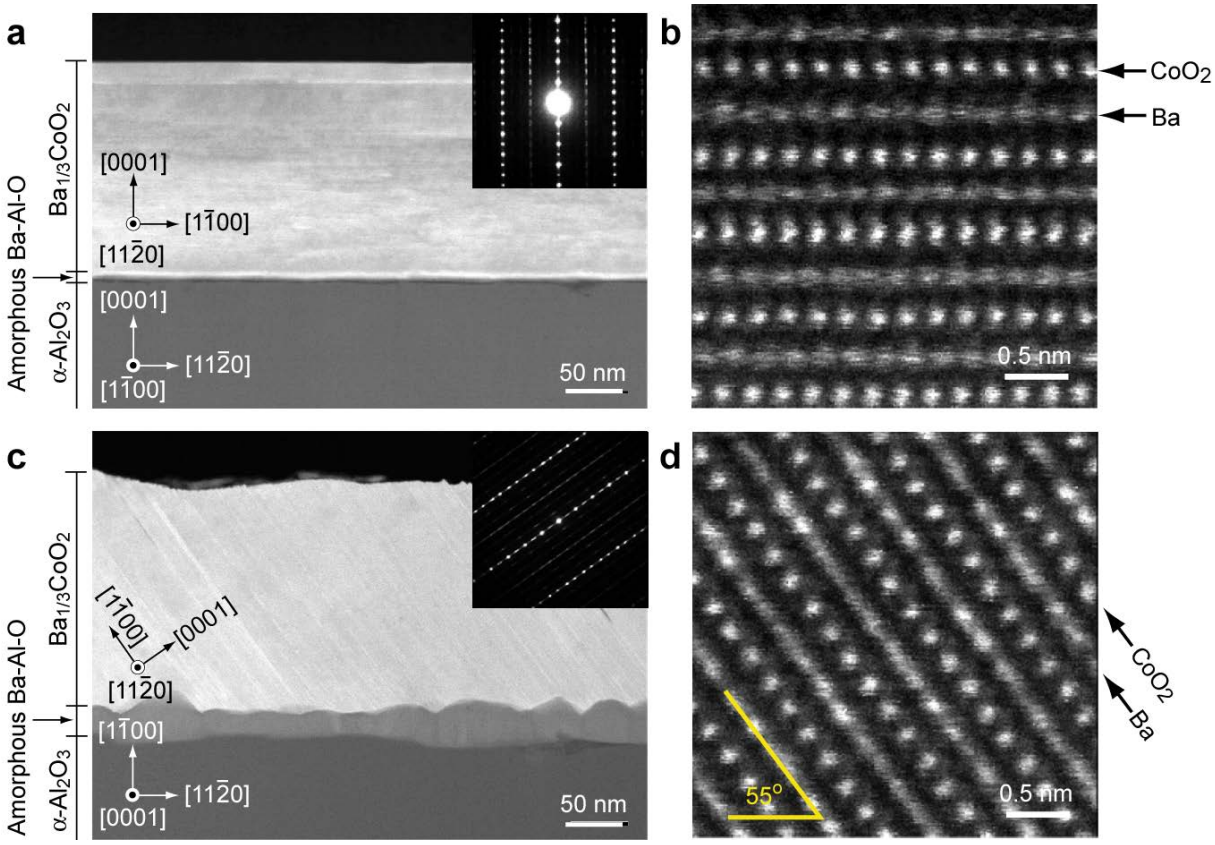

Figure 4. Cross-sectional atomic arrangement of the $Ba_{1/3}CoO_2$ films. (a) Cross-sectional HAADF-STEM image of the $Ba_{1/3}CoO_2$ epitaxial film grown on (0001) α-Al_2O_3 substrate. The selected area electron diffraction pattern and (b) the magnified HAADF-STEM image reveals that Ba and CoO_2 layers are stacked parallel to the substrate surface. (c) Cross-sectional HAADF-STEM image of the $Ba_{1/3}CoO_2$ epitaxial film grown on (1-100) α-Al_2O_3 substrate. The selected area electron diffraction pattern and (d) the magnified HAADF-STEM image reveals that Ba and CoO_2 layers are inclined 55° to the substrate surface.

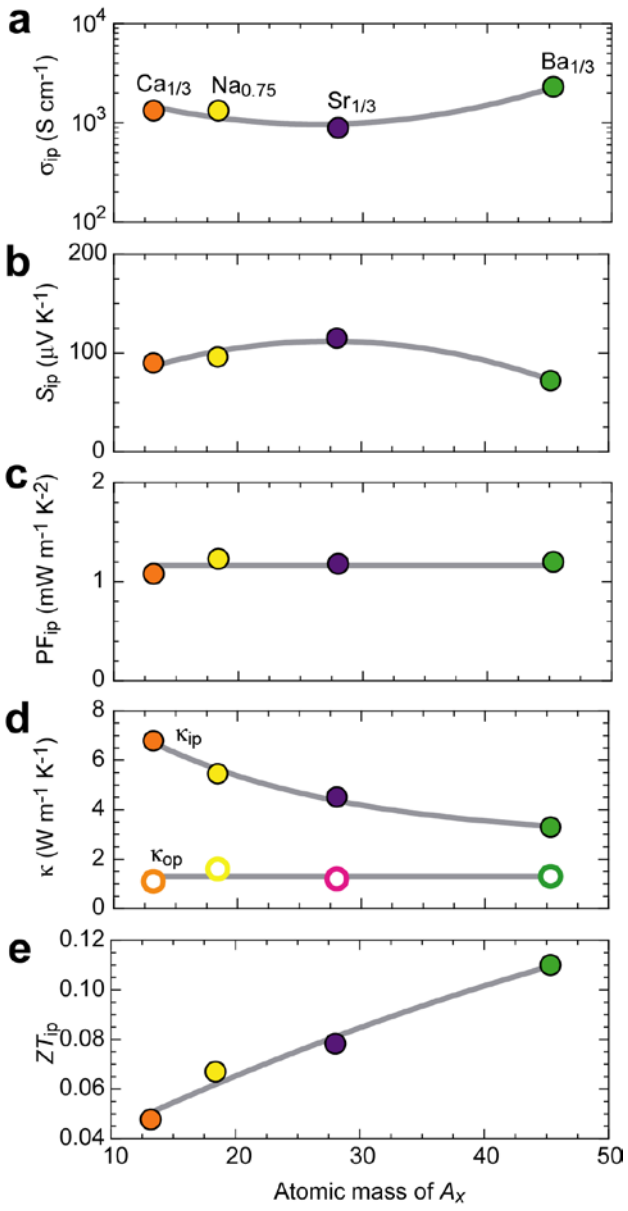

Figure 5. Thermoelectric properties of A_xCoO_2 epitaxial films at room temperature. (a) in-plane electrical conductivity (σ_{ip}), (b) in-plane thermopower (S_{ip}), (c) in-plane power factor (PF_{ip}), (d) in-plane and out-of-plane thermal conductivity (κ_{ip}, κ_{op}), and (e) in-plane figure of merit (ZT_{ip}) as a function of the atomic mass of A_x in A_xCoO_2. The κ_{ip} shows a clear decreasing tendency whereas the PF shows a slightly increasing tendency. These resulted in an increasing tendency of ZT. The ZT reached 0.11 when $A_x = Ba_{1/3}$.